SCIENTIFIC JOURNAL
EARTH'S CRYOSPHERE

Earth`s Cryosphere, 2015, vol. XIX, No. 4, pp. 84–95 **http://earthcryosphere.ru/**

METHODS FOR CRYOSPHERE RESEARCH

RESULTS OF GEOPHYSICAL SURVEYS OF THE AREA OF "YAMAL CRATER", THE NEW GEOLOGICAL STRUCTURE

V.V. Olenchenko, A.I. Sinitsky*, E.Y. Antonov, I.N. Eltsov, O.N. Kushnarenko, A.E. Plotnikov, V.V. Potapov, M.I. Epov

Trofimuk Institute of Petroleum Geology and Geophysics, SB RAS,
3 Akad. Koptyuga ave., Novosibirsk, 630090, Russia; OlenchenkoVV@ipgg.sbras.ru
** Gazprom VNIIGAZ, Razvilka village, Moscow region, 142717, Russia*

Results of the field observations and geophysical surveys of the site of recently emerged geological formation known as the "Yamal crater" have been presented and discussed. The purpose of the research was to determine its origin. In 2014, permafrost and geomorphological observations, sampling of soil and water, geodetic and geophysical surveys were carried out, which revealed the absence of radiation anomalies. It has been demonstrated that the crater is contoured by circular negative anomalies of the magnetic field, and is confined to the intersection point of linear negative magnetic anomalies. It was found that the crater occurs at the junction of geoelectrical structures, and geophysical characteristics defined for gas hydrate-bearing horizons occurring at a depth of 60–80 m. It is suggested that either deep gas migrated through faults or shallow occurring gas-hydrate decomposition could be the source of gas. The research findings have revealed that the crater was formed in the place of the preexisted pingo, and posed the problem of detecting hazardous pingos, which can be solved by integrated studies, including geocryological and geophysical surveys, and proof drilling.

"Yamal crater", pingo, permafrost, gas, gas hydrate, fault, geophysical methods, geoelectric section, electrical resistivity tomography, electromagnetic sounding

INTRODUCTION

Early in 2014 the Internet and mass media splashed photo and video materials about the stunning discovery on the Yamal Peninsula – the "mystery crater", in the vicinity of the Biovanenkovo field. The new geological formation is a circular gaping hole of impressive size in the ground, rimmed with the thrown out soils around its circumference.

The visual inspection of the object of interest on July 16, 2014 during the first expedition led by M.O. Leibman Dr. Sci. in geol.-miner., revealed that that the crater is not greater than 30 m in diameter, its depth is more than 50 m. Judging from the external examination, the crater was formed by a powerful release of gas [*Leibman and Plekhanov, 2014; Leibman et al., 2014*]. The formation of the crater in close vicinity to the Bovanenkovo oil-gas condensate field (OGCF) and the Bovanenkovo–Ukhta gas pipeline urged the study of such a phenomena as to identify the causes, hazard level, and provide insights into most probable predictable signatures of such a phenomenon. To this end, a multidisciplinary expedition was organized in the period from 13 to 18 September 2014 with the support of Gazprom Dobycha Nadym LLC, which included experts from the Trofimuk Institute of Petroleum Geology and Geophysics (IPGG) SB RAS (Novosibirsk) and the Scientific & Research Institute of Natural Gases and Gas Technologies – Gazprom VNIIGAZ (Moscow). The main purpose of the field works was to determine the nature of the geologic anomaly.

The primary goals of geophysical surveys consisted in: evaluation of geological and geohydrological structure of the area; establishing a possible association of the crater location with geophysical anomalies; determining the crater position in geophysical fields, as well as on the earth resistance maps and sections. Another important task to be solved by the deployed geophysical methods was to rule out or confirm, whether the crater origination would opt for anthropogenic or cosmogenic hypotheses.

Geomorphological structure, geological and hydrological characteristics of the study area

The study area is located in the central part of the Yamal Peninsula. In terms of geomorphology, this is a surface of erosion-accumulative plain, mostly flat, swampy, lake-studded, dissected by a network of rivers and gullies, and is polygonal structured. The abso-

lute elevations vary from 0.5–3.0 to 41–45 meters at watersheds. The plain has a two-level structure: the outliers of 3rd Marine Terrace (3rd MT) of Upper Pleistocene age and Upper Pleistocene–Holocene above floodplain terraces form the upper level, whereas flatlands of the Seyakha and Mordyyaha rivers' floodplains constitute the lower level [*Baulin et al., 1996*].

The study area falls into a typical tundra subzone, where moss-lichen-shrub and shrub and sedge-moss are most common plant-community types. The vegetation cover is dense and includes different types of sedges, cotton grass, wild grasses, and moss [*Trofimov, 1975*]. The place is abounding with thermokarst lakes, which area increased by 5 % in low and middle floodplains, and decreased by 7 % in the watershed areas over the period from 1992 to 2002 [*Sannikov, 2012*].

The geological structure of the area involves loose Paleogene–Quaternary sedimentary rocks to a depth of 500 m, mostly clay-loam–clayey in composition [*Skorobogatov et al., 2003*]. Their bottom part is represented by Paleocene–Eocene (mP_{1-2}) marine gray and dark gray clay loams with inclusions of gravel, pebbles and faunal remains, and dark gray (to black) clay with numerous remains of the marine fauna, and silt sand dustings, on average about 250 m thick. The overlying Lower–Middle Pleistocene marine deposits of the Yamalian series (mQ^{1-2}_{I-II}) are distributed throughout the entire area, with thickness reaching 120–200 m in the Bovanenkovo OGCF area. The Yamalian series deposits are represented by gray clay loams with thin interbedding of silt sand, light gray with black carbonaceous spots. Numerous gas blowouts recorded while drilling the permafrost-parametric wells while the Bovanenkovo OGCF area are commonly associated with the decomposition of relict gas hydrates commonly attributed to deposits of the Yamalian age [*Chuvilin et al., 2007*].

The basal layer of the Paleogene–Quaternary sequence comprises a thick Turonian-Maastrichtian argillaceous unit (Upper Cretaceous) underlain by Cenomanian gas-bearing deposits [*Kozlov et al., 1999; Skorobogatov et al., 2003*]. The crater is located in a well-studied inherited positive structure (South Murtinskaya), confined to Lower and Middle Jurassic deposits [*Astafiev and Skorobogatov, 2006*].

The study area is characterized by a continuous distribution of perennially frozen rock (PFR), or permafrost, which developed from the surface to a depth of 180–300 m. The thickness of permafrost strata, varying from 120 to 250 m, is largely governed by the area's geomorphology and landscape conditions [*Chuvilin et al., 2007*]. The mean annual permafrost temperature at a depth of zero annual amplitudes in the Bovanenkovo OGCF area constitutes –4...–6 °C [*Baulin et al., 1996*].

The upper part of the section is complicated by very ice rich deposits and ice soils of various forms – ice wedges and massive ground ice, with pingos sparsely scattered over the surface, both small-sized formed by first-year ice, and large perennial frost mounds produced by injection of water – bulgunnyakhs, or pingos [*Baulin et al., 1996; Dubikov, 2002*].

METHODS AND METHODOLOGY OF STUDIES

A whole complex of works – morphometric studies, soil/water sampling, geophysical surveys on the basis of radiometry, magnetic, electrical resistivity tomography (ERT) and near-field transient EM (TEM) sounding – was conducted at the Yamal crater site, in order to support or rule out the conjectures that has abounded about the crater origin.

The geological and geomorphological and landscape studies provided for: 1) determination of the crater geomorphological position, its hydrological and landscape conditions; 2) examination of the current state of the vegetation-soil cover (including that of the disturbed layers) in close vicinity of the crater; 3) geographical demarcation of the crater (GPS-survey); 4) mapping of the crater-perturbed ground zone (specifically, the range of displaced soil); 5) geodetic surveys.

Following the pre-designed scheme, the site was staked out with surface benchmarks (metal pegs) and geodetic measurements were performed with the use of GPS-receiver, LTI TruPulse 200/200B laser rangefinder, DQL-8 compass, geodesic landmarks with reflector, and a roulette.

The resulting data apart from determining the crater's key boundaries accurate positioning, and the water baseline inside the crater, provided a basis for its modeling.

The adjacent lakes depths were measured using a measuring stick and the JJ-Connect Fisherman 130 echo/depth sounder. The water temperature in the lakes was measured with a thermometer incorporated into the echo-sounder, and with electronic thermometer HOBO U12-015-02 – in the crater.

The complex of geophysical survey techniques included electrical resistivity tomography (ERT), near-field transient electromagnetic sounding (Transient Electro Magnetic (TEM) sounding), magnetic survey, and radioactivity survey.

The ERT surveys were conducted with the use of the "Tundra-48" ERT system, which actually is a modification of the "Skala-48" device designed at IPGG SB RAS [*Balkov et al., 2012*]. A dipole-dipole system (dipole size: 15 meters) was deployed with the measurements taken every 5 m along the profile, which permitted studying the section to a depth of 55 m. The ERT survey was carried out along an orthogonal network (six profiles for both sublatitudinal and submeridional directions). The profiles (475 m long each) were spaced at 25-m intervals. The ERT

profiles layout scheme is shown in Fig. 1. The data obtained were processed using the Res2Dinv, Res3-Dinv programs (Geotomo Software) [*Loke et al., 2003*].

Transient electromagnetic (TEM) surveys was carried out along the profile running through the crater (Fig. 1) (transmitter loop size: 100 × 100 m; spacing interval on the profile: 100 m). Electromagnetic field (EMF) was measured by the frame sensors sized 1 × 1 m, with magnetic moment equivalent to a single-turn loop sized 50 × 50 m. The sensors were positioned in the center of each transmitter loop, and on the profile line with spacing of 100 m. The above-crater measurements were taken from the top of the rims at three points on its western, eastern and southern sides.

The TEM measurements were made possible with the SGS-TEM systems (manufacturer: "SibGeosystems" company; www.sibgeosystems.ru/hardware/FastSnap/) and specialized software for the Fast-Snap equipment. The TEM total survey activities encompassed 20 physical observation points from 9 transmitter loops. The quantitative interpretation and analysis of the TEM survey data were conducted with the use of TEM-IP program, developed at IPGG SB RAS [*Antonov et al., 2014*]. The interpretation resulted in estimation of thickness, electrical resistivity (ER) and induced polarization (IP) parameters of the layers composing the section.

The magnetic prospecting surveys were run on an irregular observational network in the course of the "zigzag" route survey. Full magnetic induction was measured by proton Overhauser magnetometer GEM-19T (GEM Systems, Canada). The data processing consisted of daily and short-period records of MF variations for subsequent construction of the isodynamic map. The interpretation carried out on a qualitative level (qualitative data analysis) involved identification of mark-related anomalies, with assessment of their intensity, form and extent.

Natural radioactivity was measured with the use of PSA-68-01 equipment (http://ntfprompribor.ru/page145572). The radioactivity survey profile transected the study area in the sub-latitudinal direction, and its layout scheme is shown in Fig. 1. The measurements were taken along the profile with a spacing 5–7 meters, and their result were subsequently used for plotting natural radioactivity (gamma background) along the profile.

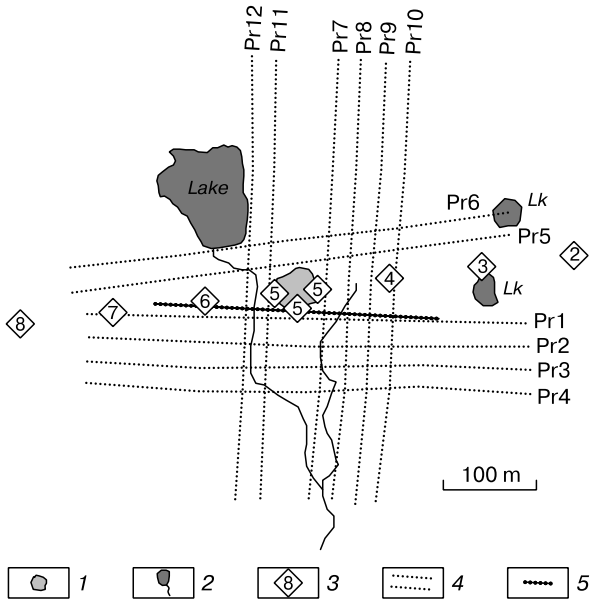

Fig. 1. Layout scheme for location of electrical resistivity tomography profile, receivers for TEM sounding and radiometric profile:

1 – crater; *2* – hydrological network; *3* – receiver; *4* – ERT profiles; *5* – radioactivity survey profile.

RESEARCH RESULTS

Geomorphological and geodetic observations

The "Yamal gaping hole" (crater) is located 39 km south of the nearest production facilities of the Bovanenkovo OGCF (well pad 610) and less than 4 km to the east of the operating Bovanenkovo–Ukhta gas trunkline system. The WGS 84 system coordinates of the crater are N69 58.280 E68 22.239 (the northern edge) and N69 58.268 E68 22.214 (its central part).

The field observations resulted in compilation of geomorphological scheme for the crater site, comprising specific cryogenic processes, attendant phenomena and landscape characteristics (Fig. 2).

Fig. 2 shows that the study area was subjected to recent (in terms of geologic time) floods, which is corroborated by characteristically high banks of the paleolake, traceable in the relief practically around the entire perimeter of the area (except for the southern part). The diameter of the preexisted paleo-lake is about 700 m, which subsequent drying is most likely to have taken place step-wise.

The fragments of a younger paleolake emplaced inside its precursor, are also fairly well expressed in the present-day relief. Shrubby vegetation (predominantly, willows) is developed along the margins, which is indicative of runoff troughs and watercourses valleys. The crater is located right there, in the southern part of the study area, at the intersection of the contemporary watercourse (stream flowing out of the lake) and the shoreline of the primordial paleolake. The creek valley appears to be a geomorphological feature of the tectonic dislocation of submeridional strike.

A small waterfall on the creek located 15 m to the west of the crater, represents the boundary of different level surfaces, which typifies geomorphological features of the tectonic contact (fault) of sublatitudinal strike [*Kostenko, 1999*].

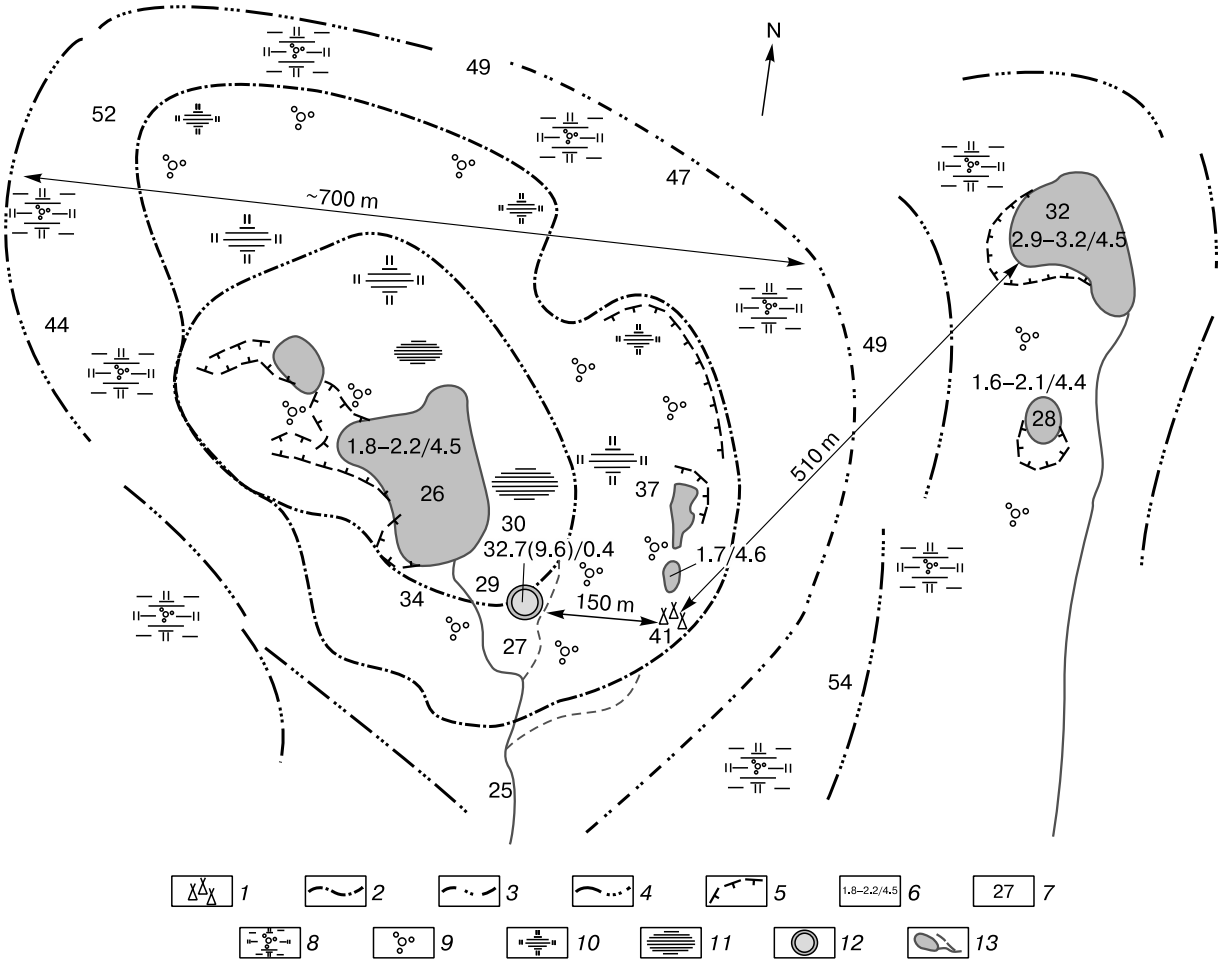

Fig. 2. Geomorphology scheme of the study area:

1 – field camp; *2* – paleo-lake shore No. 1; *3* – paleo-lake shore No. 2; *4* – water-parting lines; *5* – cryogenic landslides and creeps of ground, thermokarst; *6* – depth (m)/temperature (°C) in the lake/crater; *7* – absolute elevations of day surface; *8* – shrub, rarely moss-lichen, vegetation, pit-and-mount tundra (dwarf birch, low-bush berries, sedge, moss, lichens); *9* – shrub vegetation, run-off channels, stream flow valleys, bases of steep slopes (mixed herbs willow-shrub, dwarf birch thicket 0.5–1.0 m high, more rarely up to 2 m); *10* – moss-lichens, sedge, rarely low-shrub vegetation (bottoms of paleolakes, slopes of ravines); *11* – sedge, rarely moss-lichens vegetation, bog (bottoms of paleolakes, waterstreams channels and valleys); *12* – crater; *13* – hydrological network.

The hydrological studies of the nearby lakes revealed that they do not have any anomalous depths, which range between 1.8 and 3.2 m, depending on the size. The water temperature in the lakes averages at 4.4–4.5 °C.

When examining the site for displaced fragments of deposits and traces of impacts of the fallen massive ground ice pieces, 47 fragments were documented; their real number should have been higher, though. Dimensions of the deposit fragments (lumps of clay- and sand-loam) vary from 2 meters or more in close proximity to the crater rims up to 0.2 m in the periphery part. The displaced fragments of deposits and ice are recorded around the crater perimeter, with the radius of their spread exceeding 160 m.

Relying on the visual examination results, the crater can be described by the following structural characteristics: the deposits displaced by the blowout made up a rim around the funnel circumference with a height ranging from 1 to 4 m. The upper part of the crater section, to a depth of 2–3 m, is represented by ice-rich sand-loam and argillaceous rocks (Fig. 3). The crater has a funnel with walls descending at a negative angle. All the visible part of the vertical section, except for the first 2.5–3.0 meters, is composed of ground ice which layers occur with angular unconformity with the overlying sediments. A flat-lying lens of milky-white ice is also exposed in the crater wall.

The bottom part of the crater is filled with melted water, very muddy, abounding with suspended

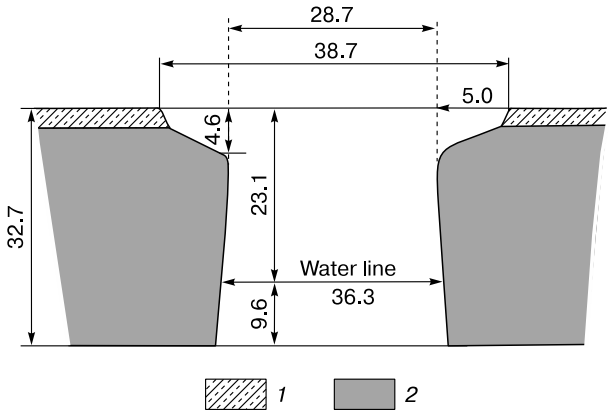

Fig. 3. Schematic section of the crater (sized in meters):

1 – sand- and clay-loams; *2* – massive ground ice.

clay particles, with a "coat" of fragments of roots and plant remains floating on the water surface. On the north-eastern side, a fairly large thawed niche is clearly visible at the water line interface in the lower part of the crater funnel. The upper edge of the niche was located at a depth of 16.5 m from the day surface at the time of the study.

The soil, deposits, water samples from the crater and its adjacent area were studied at the laboratory for chromatographic analyses at the Engineering and Technical Center of "Gazprom Dobycha Nadym". The results analysis showed no anomaly in the content of various components in the soil samples from the crater rims and the surrounding area.

The compositions of water samples from the crater and the lakes differ due to higher concentrations of hydrogen ion (166 mg/m^3) in the crater water compared to that of lake water (22–42 mg/m^3), and because of the presence of oil admixture (1.31 mg/m^3 on the background of 0.16–0.22 mg/m^3), and copper (0.0081 mg/m^3), manganese (0.48), mercury ($4 \cdot 10^{-5}$), phenols ($5.4 \cdot 10^{-3}$), anomalous concentrations of nitrate ion (10.24) and nitrite-nitrogen (0.02 mg/m^3). Electrical conductivity of the crater water is 395 μS/cm, and 120–310 μS/cm that of the nearby lakes water. COD (chemical oxygen demand) was found also abnormally high – 7017 mgO_2/L in crater water versus 40–63 mgO_2/L in lake water. COD is an indicator of total content of organic substances in water in terms of the amount of chemically bound oxygen consumed by the oxidation processes. A large fallen off fragment of top-soil and sand-loam/clay-loam deposits with a lot of plant residues are assumed to be the main source of organic matter in the crater water.

A more detailed characterization of the crater relief and structure is provided in [*Kizyakov et al., 2015*].

The diverse chemical compositions of the two waters is accounted for the fact that the crater is filling with water streaming down from the thawing ice walls as well as with surface water running over the crater rims, whereas the lakes appear to be replenished mainly by the atmospheric precipitation. The deposits samples from the crater rim and the surrounding area showed the presence of copper (24–86 mg/kg) and oil admixture (6–198 mg/kg), which allows an inference about these elements getting into the crater water from the surface at the expense of the collapsed crater rims.

Results of geophysical surveys

Fig. 4, *a* shows a contour map of the increment of full vector of magnetic induction (isodynamic map). The magnetic field varies within a narrow range from –11 to +13 nT. The crater is located in the zone of intersection of linear NW–NE trending negative anomalies of the magnetic field. The anomalies extents coincide with the dominant strike of faults in the study area [*Podurushin, 2011*]. Therefore, the magnetic field anomalies can be associated with supergene alteration of rocks in the fault zone caused by the oxidation of accessory magnetic minerals and their conversion to non-magnetic minerals.

A local intense negative anomaly, located 20 meters south of the crater is related to the metal pins (fixing device of climbing insurance, left behind by the forerunner expedition).

The right bank of the creek (western part of the site) is found in negative magnetic field. This zone is supposedly of submeridional, close to N–NW strike. Negative magnetic field in western part of the site can be associated with the zone of tectonic dislocations trending north-northwest (N–NW).

A three-dimensional (3D) isodynam surface shows that the crater is confined to the isometric negative anomaly (about 100 m in dia) of magnetic field and this anomaly, in turn, gravitates to the intersection point of assumed faults (Fig. 4, *b*). Being isometric in plan, the negative anomaly of magnetic field can be accounted for the presence of vertical channel for hydrocarbons migration to the surface [*Bezukladnov and Mavrichev, 1997*].

Thus, according to the magnetic measurements the crater is situated in the local isometric negative anomaly of magnetic field. The crater is confined to the intersection point of linear negative anomalies trending NE and N–NW, which fragments were identified by the magnetic surveys. The linear anomalies of MF trending coincides with general strike of the fault system.

The absence of intense anomalies of magnetic field characteristic of large iron objects (such as a meteorite), allows to basically ignore the cosmogenic nature of the crater, since it is known that iron and iron-stone meteorites account only for 7.2 % of the

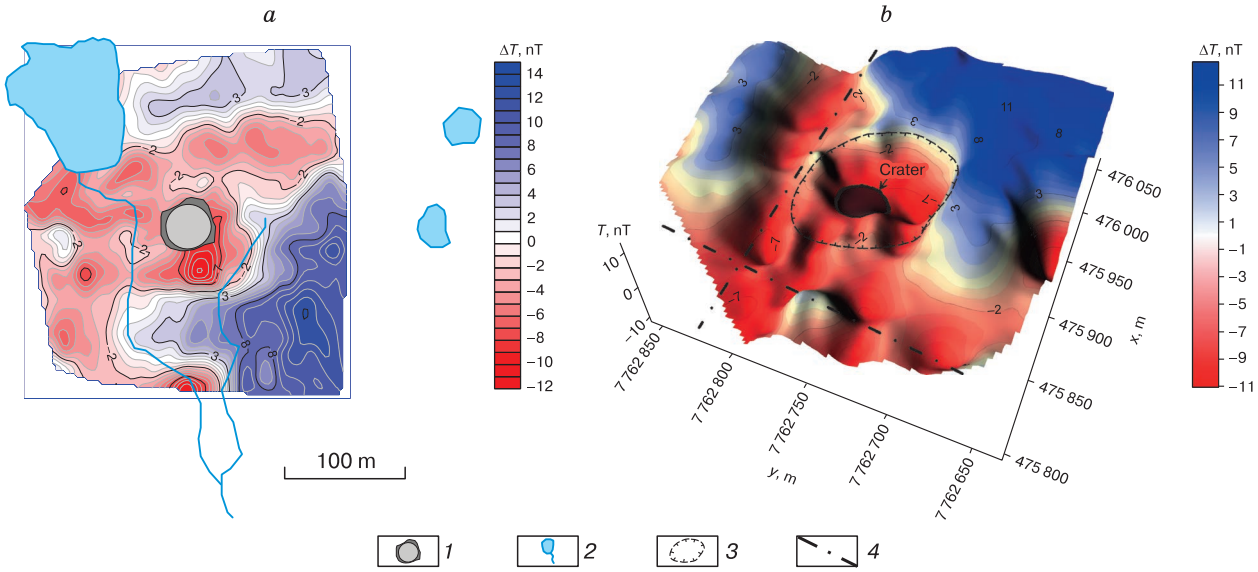

Fig. 4. A map (*a*) and surface (*b*) of increment of full vector of magnetic induction (Δ*T*):

1 – crater; *2* – hydrological network; *3* – contoured isometric negative anomaly Δ*T*; *4* – axes of linear negative anomalies Δ*T*.

total number of meteorites falling onto the Earth (www.meteorites.ru/kr_o_met.html). Despite the negligible amount of the latter (percentage), this does not allow to completely rule out the impact hypothesis, in the absence of other information.

Measurements of the gamma background did not record any significant anomalies within the site. Similar inferences were made on the basis of measurements taken on July, 16 2014, i.e. early in the first summer of the existence of the crater funnel [*Leibman and Plekhanov, 2014*]. The radiation field intensity, according to our data, varies from 7 to 11 μR/h. It slightly increased in the background, though, within the study area due to the lack of moss on the crater rims. Minimal radiation values are observed above watered areas of the profile.

Results of ER tomography

Statistical processing of the ERT data showed that the rocks identified in the massif fall into three groups differing in electrical resistivity (Fig. 5). According to the known ER dependencies on temperature and lithology [*Vakhromeev et al., 1997; Frolov, 1998; SP 11-105-97..., 2004*] at a temperature of –5 °C typical for the depth of zero annual fluctuations in the study area [*Baulin et al., 1996*] rocks with ER about 250 Ohm·m correspond to frozen clay-loam.

The 1350 Ohm·m peak in the histogram accounts for sand-loam, whereas ice is responsible for the highest ER values (tens of thousands of ohms per meter). The criteria for the geological interpretation of geoelectric sections have thus been established, those in good agreement with the data for the structure of the study area [*Chuvilin et al., 2007*].The modal ER values derived from statistical analysis should not be applied dogmatically to the interpretation of electrical prospecting data.

Any rise in ice content of rocks leads to a significant increase in their resistivity, whereas a rise in salinity, on the contrary, greatly reduces electrical resistance. Therefore, ER values employed by different petrophysical groups tend to overlap.

Fig. 6, *a* and *b* show the geoelectric sections on Profile lines 1 and 7, respectively, located approximately 15 meters from the southern and eastern sides of the crater. On the sections, zones with lower ER

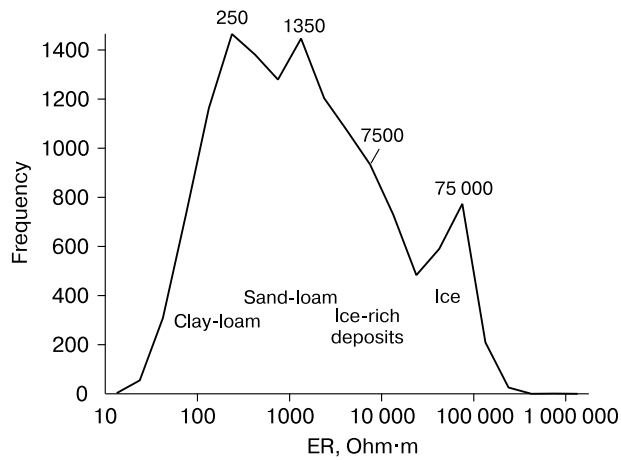

Fig. 5. Histogram for electrical resistivity distribution of geoelectric models in the study area (from results of two-dimensional inversion).

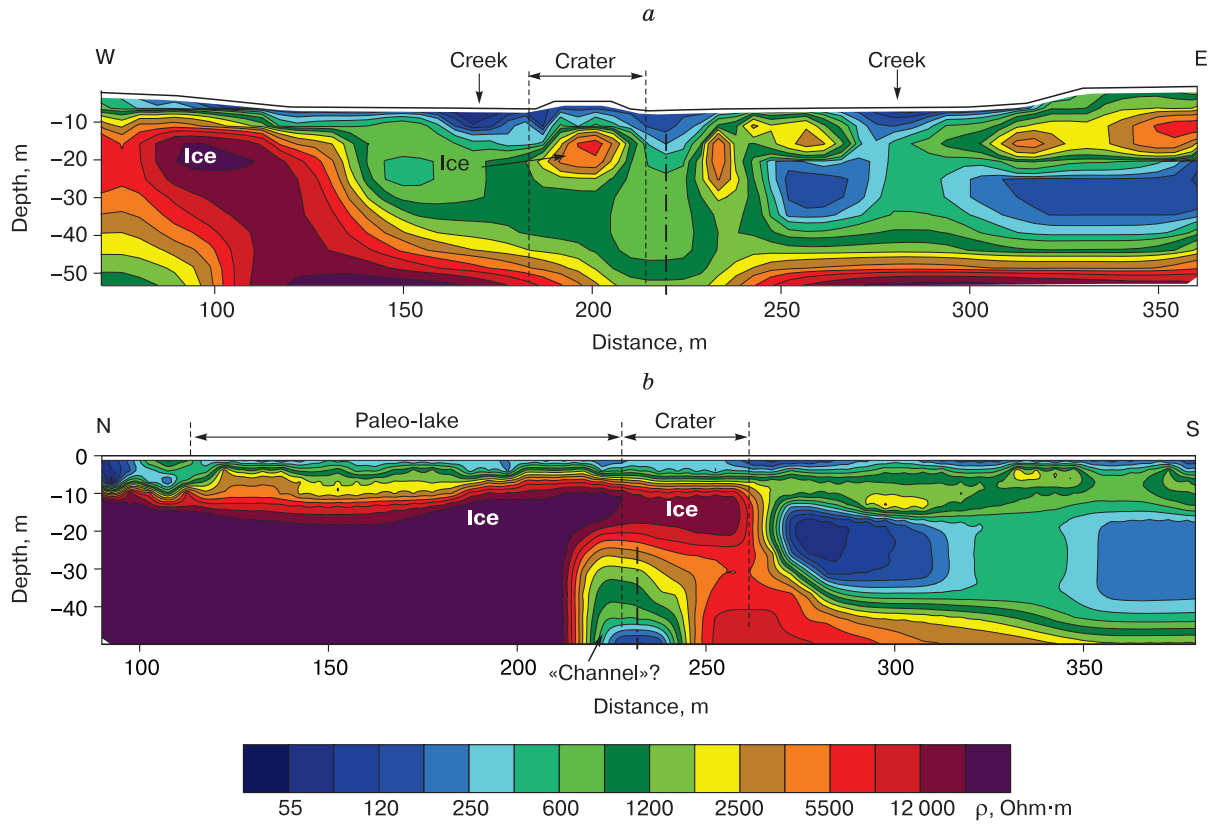

Fig. 6. Geoelectric sections along profile 1 from southern (*a*) and profile 7 from eastern (*b*) sides of the crater.

Dot-and-dash lines – axis of vertical low ER anomalies.

(100–250 Ohm·m) correspond to frozen clay-loams, whereas zones with ER exceeding 2000 Ohm·m are interpreted as ice-rich rocks and ice.

Along profile line 1, a subvertical zone of reduced ER about 30 m thick is identified to the right of the crater projection on the section (Fig. 6, *a*). Despite the fact that the crater walls to a visible depth (23.1 m) abound with ice (Fig. 3), it is clearly seen from southern side of the geoelectric section that the ice-related anomaly is of local scale, and that the massive icy bed is not continuous in the upper part of the section on the southern side of the crater (Fig. 6, *a*). A massive ice body with non-identifiable lower boundary is discriminated in the section along profile 7 (eastern side of the crater) within the bounds of paleo-lake from a depth of about 10 m (Fig. 6, *b*). The masking effect does not allow electric current to flow through the insulator layer (ice) in the presence of watered low resistance layer (water) on the swampy surface.

Thickness of massive ground ice near the crater correlates with the thickness of high-resistance layer, which is found to be about 18 m. In the middle part of the profile (in the 230–260 m interval) a vertical anomalously low ER zone (less than 500 Ohm·m) is discriminated at a depth of 30–50 m, with its 30 m horizontal thickness. Probably, this is related to an anomaly associated with a (thawed?) feeder channel through which gas migrated to the surface. However, the presence of a thawed channel is yet to be proved by thermometric methods.

Given that there's a remarkable mismatch between geoelectric models in the profiles intersection point (the 220 m picket on profile 1 corresponds to the 280 m picket on profile 7), this can be explained by the fact that geoelectric sections are derived from 2D inversion, which assumes that the medium is two-dimensional; in reality, the subsurface medium of the study area is a complex 3D object. At solving the inverse problem within the scope of 2D model the sections tend to be influenced by 3D geological inhomogeneities.

The profile's position in relation to the inhomogeneities will largely control the resulting 2D geoelectric model. Therefore, any mismatch of geoelectric sections in the profile intersection points stems from a 3D subsurface medium, in the first place. In order to ultimately understand the geological medi-

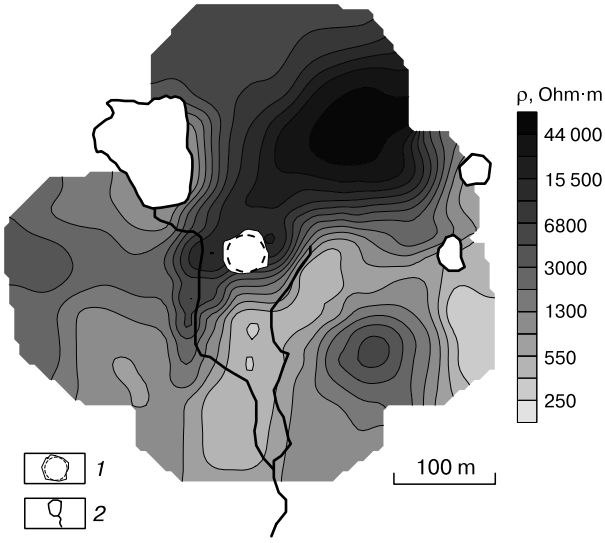

Fig. 7. A map of electrical resistivity distribution at a depth of 30 m:

1 – crater; *2* – hydrological network.

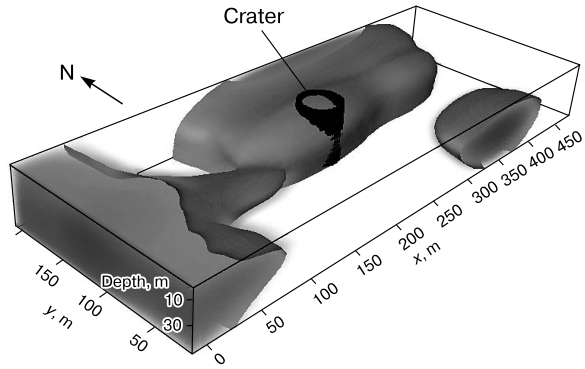

Fig. 8. Geoelectrical 3D model of the medium.

Non-transparent areas – rocks with ER exceeding 2000 Ohm·m.

um a 3D inverse problem is to be solved, resulting in the construction of a volume model. However, given that it is generalized, minor details are largely neglected, which could be discerned in the previous 2D sections. 3D geoelectric modeling provides a general characterization of ER distribution in the medium.

Fig. 7 shows an ER distribution map representing a 30 m depth slice of the 3D model. The northern part of the site is characterized by high ER values (7000–100 000 Ohm·m), which is associated with the extent of massive icy bed within the paleo-lake area. To the south of the crater, occurs a lower ER (250–800 Ohm·m) linear zone of submeridional strike. This zone is spatially coincides with the creek valley, and may be indicative either of lower ice content in the deposits, or greater clay content.

The ER distribution map shows that the crater occurs unconformably in relation to the geoelectric structures and is not confined to any one of the identified anomalies, and rips through geoelectric boundaries. However, it is very much likely that the mesh detail level during construction of 3D geoelectric model appears not sufficient to ascertain the influence of the crater and feed channel on ER distribution in the medium.

The 3D model of ER distribution in the surrounding medium is shown in Fig. 8. Very ice-rich rocks and ground ices were defined by the 2000 Ohm·m ER isosurface. The model explicitly demonstrated that the crater formation took place in the marginal part of the high-resistivity sedimentary complex. Massive ground ice is probably absent from the southern side of the crater.

The ERT surveys data allowed the following conclusions: geoelectric structure of the site being extremely inhomogeneous, this may have been caused by different ice content and lithologies of rocks; geoelectric sections of the southern and eastern sides of the crater display vertical lower ER anomalies with horizontal thickness of about 30 m; to the south of the crater, a linear zone of lower ER values of submeridional strike is identified. The crater occurs unconformably with geoelectric structures at the interface between rocks with high and low resistivity.

Near-field transient electromagnetic sounding

According to TEM surveys, resistivity section to a depth of 200 m across the study area is approximated by a four-layer structure (Fig. 9). Resistivity of the first subsurface layer equals to 246–445 Ohm·m, its thickness varies between 50–65 m. The IP parameter – chargeability (*m*) of the first layer ranges from 0.12 to 0.27. At this, the contact boundary between rocks with high (0.27) and low (0.13) chargeability is observed in the crater.

The second layer is characterized by abnormally high ER 400–880 Ohm·m, its thickness ranges from 7.5 to 20 m. In the 55–80 m depth interval, occurs anomalously high-resistivity horizon (7.5–11.0 Ohm·m) with great thickness (70–100 m). Typically, TEM measurements provide data allowing to identify with high accuracy the top of conductive layer, and thus defined depth of the detected low-ER horizon is considered reliable. The underlying layer occurring at a depth of 135–190 m has even lower ER values (3.4–5.1 Ohm·m), whereas the low ER values (3–10 Ohm·m) are accounted for the deposits salinity.

The geoelectrc section analysis has shown that the crater is located at the boundary between two geoelectric structures. Unlike eastern, the western part of the section is characterized by higher ER in the first layer. In the crater area, the lowest ER values are marked both from western and eastern sides,

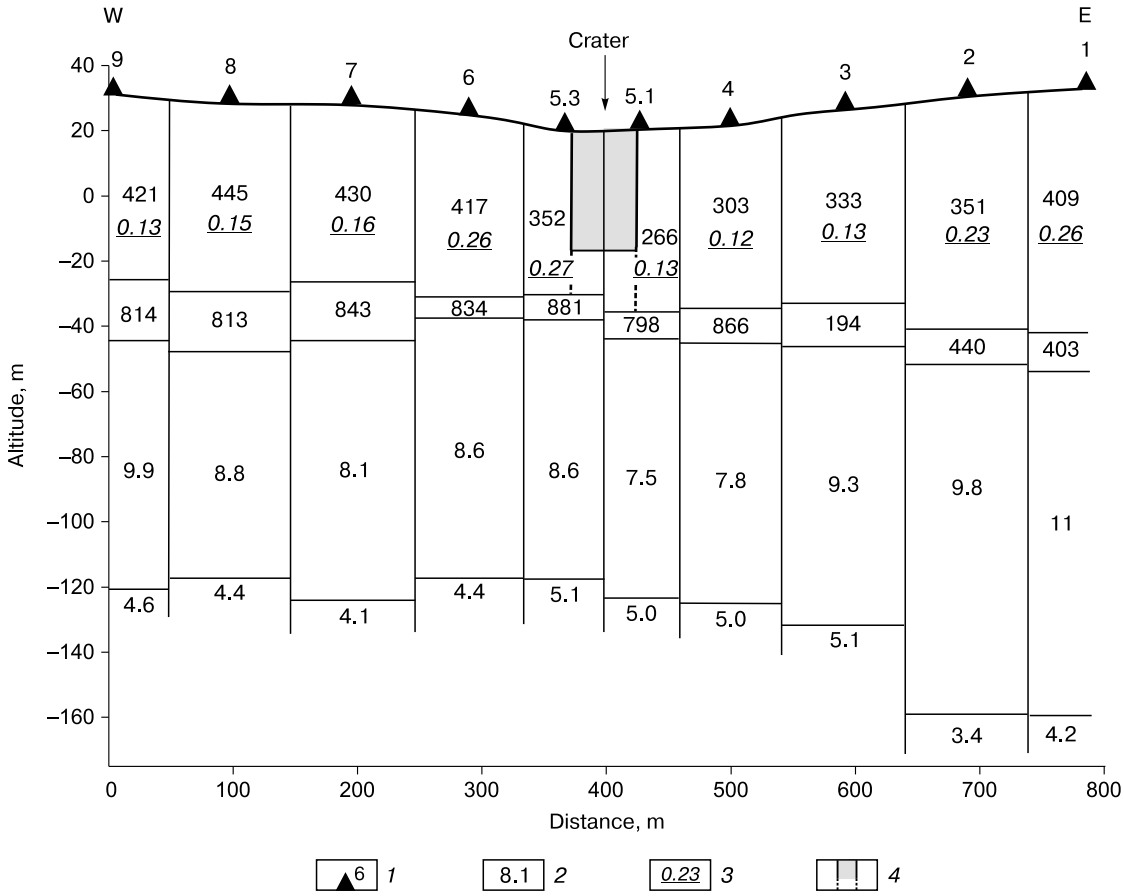

Fig. 9. Geoelectric section from TEM sounding (near-field transient electromagnetic sounding) data:

1 – TEM measurement points; *2* – electrical resistivity of rocks, Ohm·m; *3* – chargeability of rocks, u.f.; *4* – the crater projection on section.

which is indicative of a fault zone. ER diagram for the first layer on the resistivity expansion profile is shown in Fig. 10. The lowest resistivity is expressed in the diagram for the central part, which indicates to the presence of contact between the geoelectric structures in the place where the crater subsequently formed.

Elevated ER and chargeability of the first layer account primarily for enhanced ice content in the upper part of the section and for the presence of massive ground ice. In this case, it appears extremely challenging to delineate a massive ice body using TEM method due to immanent characteristics of the latter.

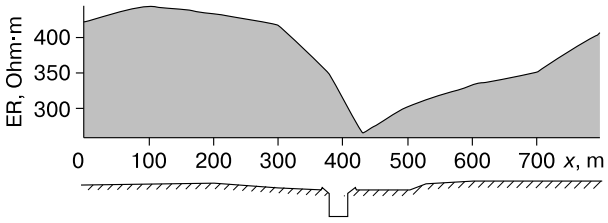

Fig. 10. Diagram of electrical resistivity of the first layer along the TEM soundings profile.

A thin layer with abnormally high ER values (400–880 Ohm·m) is defined in the 60–80 m depth interval. The anomaly can be explained by high ice content in the deposits and abundant inclusions of relict gas hydrates (methane clathrates). Typically, gas hydrates occur in reservoirs, or horizons, with interbedding of low salinity sand or sand-loam [*Chuvilin et al., 2007*]. Such factors as subsequent sanding of the section, lowering of salinity and the presence of gas hydrates will spark a dramatic increase in ER of the layer, which is probably observed on the TEM data-based geoelectric sections.

The literature data analysis revealed that within the Bovanenkovo OGC area, gas liberations caused by gas hydrates decomposition, are most frequently encountered at depths between 60 and 80 m [*Chuvilin et al., 1999, 2007*]. That is, the location of layer with abnormally high ER values in the sedimentary strata correlates with the depth of maximum gas showings in the Bovanenkovo OGC section.

The underlying layer of deposits with ER equal to 7.5–11.0 Ohm·m is interpreted as frozen Lower–Middle Pleistocene marine deposits of the Yamalian series. According to the drilling data for the Mordy-yaha river alluvial floodplain (BH 610-P-3), these are clay-loams with massive cryotexture; the permafrost base was penetrated at a depth of 165 m [*Chuvilin et al., 1999*].

The conductive layer top is identified on the geoelectric section at a depth of 135–190 m, which can be interpreted as water – ice-in-soil interface, i.e. the base of permafrost strata. Due to the fact that the boundary curve for saline marine clay-loam and clay does not coincide with the zero-isotherm, the lower limit of the occurring deeper perennially frozen rocks (PFR) is not identified in the resistivity survey data.

Fig. 11 represents a geological interpretation of TEM resistivity section, providing correlated geoelectric and geologic boundaries, and showing assumed axis of tectonic faults and the water–ice phase boundary. Tectonic dislocations are marked in places of the geoelectric model type replacement, which is evidenced by sharply changing layers thickness or their ER values in the section.

The applied TEM sounding method allowed the following inferences: the upper part of the section has a high resistivity to a depth of 60–80 m, which is typical for very ice-rich PFR and massive ice bodies; the crater is located in the junction zone of geoelectric structures; a gas hydrate saturated horizon is assumed to be in the 60–80 m depth interval; the water – ice phase transitions boundary is identified at a depth of 135–190 m.

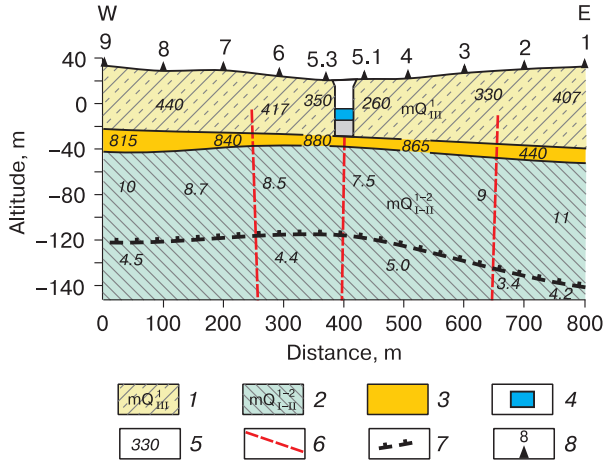

Fig. 11. Geological interpretation of geoelectric section on the basis of TEM sounding data:

1 – very ice-rich sand- and clay-loams with massive ground ice; *2* – clay-loam, Lower–Middle Pleistocene marine deposits of the Yamalian series; *3* – trapped gas hydrates; *4* – water in the crater; *5* – electrical resistivity of rocks; *6* – fault; *7* – lower boundary of perennially frozen rocks; *8* – transient electromagnetic measurement point.

DISCUSSION OF RESULTS

Results of the integrated geological and geophysical studies have shown that "the Yamal crater" is a natural geological structure. At the same time, neither its origin nor formation mechanism have thus far been clearly understood. Natural gas liberation from the permafrost appears the most probable driving mechanism of its formation. The same conclusion was reached by its pioneer researchers [*Bogoyavlenskii, 2014a,b; Leibman and Plekhanov, 2014*]. However, the source of gas that generated the excessive pressure has hitherto not been ascertained.

Analysis of high-resolution satellite imagery showed that the primordial crater locality had been occupied by almost perfectly round frost mound, 45–58 m in diameter, at its base [*Kizyakov et al., 2015; Satellite imagery..., 2015*]. The positive form of terrain may have been imparted by the long-existed forces acting from beneath.

In the course of the integrated research it has been established that:

(1) – in terms of geomorphological features (creek valley, multilevel surface) the crater is confined to the intersection point of tectonic dislocations of meridional NE and NW strikes. The presence of faults is supported by geophysical features: negative anomalies of the magnetic field, lower ER lineaments according to ERT data, contact of geoelectric structures in the crater area on the TEM section, and decreasing thickness of PFR strata.

(2) – in the section of sedimentary strata, a thin horizon with anomalously high resistivity was identified in the 60–80 m depth interval. That same depth interval is associated with most often occurring relic methane hydrate showings within the Biovanenkovo field area [*Chuvilin et al., 2007*].

(3) – based on the results, a boundary interpreted as water – ice phase transition interface is identified at a depth 135–190 m. This boundary detected immediately beneath the crater has the shallowest occurrence depth.

(4) – the analysis of geological information showed that the crater is located on the positive geological structure (South Murtinskaya) prospective for hydrocarbons (gas).

(5) – there used to be a pingo some 30 m in diameter, in the place of the presently gaping crater.

All these facts support the crater formation driven by the endogenous factors. Earlier, the authors proposed a most probable scenario of the crater formation, which involved the following conjecture: an inflated heat flow above the hydrocarbon deposits trapped in the permafrost caused destruction of the relict gas hydrates, with the reservoir pressure growing in the upper part of the section, while the top-soil destruction and displacement occurred in the most

weakened zone – at the intersection point of tectonic faults [*Epov et al., 2014*]. However, taking into account the published data [*Leibman and Plekhanov, 2014; Leibman et al., 2014; Kizyakov et al., 2015*], our views on its origin have been corrected.

The two versions of possible sources for pneumatic (pressurized) gas ejection are considered: 1) according to the first (deep gas) version, the crater is positioned above oil and gas-bearing structures, the permeable zones (faults) of which favored the upward migration of hydrocarbon gases. Typically, increased heat flow and hydrocarbons migration to the surface through the permeable zones (faults) are observed above the hydrocarbon (HC) accumulations [*Mekhtiev et al., 1971*]. This process produce a decreasing effect on the thickness of frozen rocks overlying the hydrocarbon accumulations [*Diakonov, 1958; Fotiev et al., 1974; Vozhov and Surnin, 1982*]. The permafrost thickness thinning in the study area was corroborated by the TEM survey data. Our speculation is that the migrating gas would accumulate in the interpermafrost talik beneath the freezing through paleo-lake, and the pingo could thus have formed because of the excessive pressure created there.

The second conjecture [*Leibman and Plekhanov, 2014; Leibman et al., 2014*], which we also do not rule out, deals with the avalanche decomposition of methane hydrates as a probable source of gas pressure growth, which resulted in a gas blowout ripping through the surface layer. According to M.O. Leibman, a rise in temperature of frozen soils observable in recent decades due to climate warming may have triggered the process of gas hydrates decomposition. Relying on the geophysical data obtained, we have specified the properties of gas hydrate-bearing horizons. In order to give an unambiguous answer to the question as to the presence of gas hydrates in the section, the dedicated drilling operations will be required.

In the report of experts from Engineering and Technology Center of "Gazprom Geologorazvedka" (Tyumen) presented on November, 28 2014 at the Institute of Environmental Geoscience (Moscow), it was pointed out that according to the seismic survey data, vertical anomalies of fault type going 3–5 km deep down have formed beneath many pingos, and virtually all khasyrey systems are located in these anomalous zones. The researchers do not leave out a possibility of pingos formation at the expense of deep gas migration to the surface [*Smirnov, 2014*].

The classical "frost heave – pingo" formation mechanism associated with the talik freezing through beneath the drained or dry lake can not be ignored, either [*Dostovalov and Kudryavtsev, 1967*]. When cryogenic pressure in the closed system becomes greater than the overburden resistance to tensile stress, an explosion will take place either with water outpouring onto the surface, or with gas liberation into the atmosphere [*Bogomolov and Sklyarevskaya, 1969; Danilov, 1990*]. In our case, a frost mound was located in the marginal part of the freezing paleolake. The interpermafrost talik is likely to have trapped gas migrating from the depths, and given the rise in the frozen rocks and ground ice temperature, their strength properties gradually declined [*Tsytovich, 1973*], which led to the explosion.The papers [*Bogoyavlenskii, 2014a,b*] points up that the emergence of "sinks", similar to the "Yamal crater", is not a rare phenomenon (in terms of geologic and real timescale). As a rule, any subsequent gas release is marked in the terrain by a growing pingo. It is important to learn to discern between a pingo of classical nature – the one developed due to frost heaving – and a pingo, formed as a result of gas migration.

It's been thus far unclear, whether it is possible to provide any operational forecast of pingo explosion, or if any engineering measures to prevent the explosion can be taken. There is no single correct definition of sources of gas, as to whether their nature is deep occurrence or they are formed during decomposition of relic gas hydrates in the shallow subsurface. To answers these questions we need integrated geological and geophysical studies in the areas of existing craters, pingos and ultra-deep lakes, including ice and soil sampling for detailed analyses.

CONCLUSION

The research conducted allowed us to ascertain that the "Yamal crater" is a natural geological formation, which formation may have been conditioned by natural gas release. The crater is located within the negative terrain, in a creek valley on the paleolake shore. It actually has displaced its precursor pingo. In terms of geographical positioning, the crater is located in the negative anomaly of the magnetic field, at the boundary between rock masses with high and low electrical resistivity. The background radiation has shown no significant anomalies. The electrical resistivity tomography data evidence that massive ground ice is developed in the area to the north of the crater. To the south, a low resistivity linear zone of submeridional strike extends along the creek valley. According to the EM soundings, a layer with inclusions of gas hydrates is assumed at a depth of 60–80 m, with the base of permafrost strata identified at a depth of 135–190 m. However, such interpretation of geophysical data requires proof-of-concept tests drilling.

The causes of formation of the crater are limited by two principal hypotheses. According to the first, it is the migration of gas from deep gas-bearing deposits and its accumulation in the interpermafrost talik beneath the paleo-lake, followed by a gas release. The second hypothesis deals with the overpressure developed as a result of the relic gas hydrates decomposi-

tion, caused by the permafrost warming. It must be admitted that thus far the research results have not provided an unambiguous answer to the question of the crater origin.

The authors would like to thank S.N. Menshikov, Director General of Gazprom Dobycha Nadym LLC, A.B. Osokin Deputy director of Engineering Center of Gazprom Dobycha Nadym LLC and all the staff for their help in organizing and conducting the expedition.

References

Antonov, E.Yu., Kozhevnikov, N.O., Korsakov, M.A., 2014. Automated system for interpretation of induction impulse log data, with double induced polarization taken into account. Geologia i Geofizika, 55 (8), 1282–1293.

Astafiev, D.A., Skorobogatov, V.A., 2006. Tectonic control of hydrocarbon-bearing potential of the Yamal peninsula. Geologia Nefti i Gaza, No. 2, 20–29.

Balkov, E.V., Panin, G.L., Manstein, Yu.A., et al., 2012. Electrical resistivity tomography: instruments, methodology, experience in application. Geofizika, No. 6, 54–63.

Baulin, V.V., Aksenov, V.I., Dubikov, G.I., 1996. Geotechnical Monitoring of the Yamal Oil and Gas Fields Development. V. II. Geocryological Conditions of Bovanenkovo field. IPOS SO RAN, Tyumen, 240 pp. (in Russian)

Bezukladnov, V.A., Mavrichev, V.G., 1997. Detection of "deposit" type anomalies in the magnetic field. Geologia Nefti i Gaza, No. 6, 25–29.

Bogomolov, N.S., Sklyarevskaya, A.N., 1969. On hydrolaccolith explosions in southern Chita Oblast. Naledi Sibiri: Sb. statei. Nauka, Moscow, 127–130.

Bogoyavlenskii, V.I., 2014a. Threat from catastrophic gas releases from the Arctic permafrost. Burenie i Neft, No. 9, 13–18.

Bogoyavlenskii, V.I., 2014b. Threat from catastrophic gas releases from the Arctic permafrost. Craters in Yamal and Taimyr. Part 2. Burenie i Neft, No. 9. URL: http://burneft.ru/archive/issues/2014-10/1 (submittal date: 13.03.2015).

Chuvilin, E.M., Perlova, E.V., Baranov, Yu.B., 2007. Structure and Properties of Perennially Frozen Deposits of Southern Part of the Bovanenkovo Oil-gas-condensate Field. GEOS, Moscow, 137 pp. (in Russian)

Chuvilin E.M., Yakushev, V.S., Perlova, E.V., et al., 1999. A gas constituent of the frozen strata within the Bovanenkovo oil-gas-condensate field (Yamal Peninsula). Dokl. AN SSSR, 369 (4), 522–524.

Danilov, I.D., 1990. Underground Massive Ice. Nedra, Moscow, 137 pp. (in Russian)

Diakonov, D.N., 1958. Geothermics in Petroleum Geology. Gostoptekhizdat, Moscow, 277 pp. (in Russian)

Dostovalov, B.N., Kudryavtsev, V.A., 1967. General permafrost study. Moscow University Press, Moscow, 403 pp. (in Russian)

Dubikov, G.I., 2002. Composition and cryogenic structure of frozen strata of Western Siberia. GEOS, Moscow, 246 pp. (in Russian)

Epov, M.I., Yeltsov, I.N., Olenchenko, V.V., et al., 2014. Bermuda Triangle in Yamal. Science Firsthand, No. 5 (59), pp. 14–23.

Fotiev, S.M., Danilova, N.S., Sheveleva, N.S., 1974. Geocryological conditions of Central Siberia. Nauka, Moscow, 148 pp. (in Russian)

Frolov, A.D., 1998. Electrical and elastic properties of frozen soils and ice. ONTI PNTs RAN, Pushchino, 515 pp. (in Russian)

Kizyakov, A.I., Sonyushkin, A.V., Leibman, M.O., Zimin, M.V., Khomutov, A.V., 2015. Geomorphological conditions of gas release-driven formation of crater and this form dynamics in the central Yamal. Kriosfera Zemli XIX (2), 15–25.

Kozlov, E.P., Cherdantsev, S.G., Yumachikov, F.S., 1999. Geological structure and mineral resources of the western Yamal peninsula. Additional site exploration Report, R-42-VII-IX, XIV-XV sheets; scale factor: 1:200 000. Bovanenkovo field. Tyum. br. "TFGI for the Ural Federal District ". Tyumen, 269 pp. (in Russian)

Satellite image. URL: https://www.here.com/?map=69.97111,68.37042,19,satellite&msg=Ямальский%20район (submittal date: 07.02.2015).

Kostenko, N.P., 1999. Geomorphology. Moscow University Press, Moscow, 379 pp. (in Russian)

Leibman, M.O., Kizyakov, A.I., Plekhanov, A.V., Streletskaya, I.D., 2014. New permafrost feature – deep crater in Central Yamal, West Siberia, Russia, as a response to local climate fluctuations. Geography, Environment, Sustainability, 7 (4), 68–80.

Leibman, M.O., Plekhanov, A.V., 2014. The Yamal crater – gas release funnel: results of preliminary studies. Kholod'OK, No. 2 (12), 9–15.

Loke, M.H., Acworth, I., Dahlin, T., 2003. A comparison of smooth and blocky inversion methods in 2D electrical imaging surveys. Explorat. Geophys. 34, 182–187.

Mekhtiev, Sh.F., Mirsadzhanzade, A.Kh., Aliev, S.A., 1971. Geothermal Studies of Oil and Gas Fields. Nedra, Moscow, 215 pp. (in Russian)

Podurushin, V.F., 2011. Tectonics of basement and its influence on the formation of oil and gas potential of the Yamal peninsula. Vesti Gaz. Nauki, No. 3 (8), 65–72.

Sannikov, G.S., 2012. Cartometric studies of thermokarst lakes in the area of Biovanenkovo field, Yamal peninsula. Kriosfera Zemli XVI (2), 30–37.

Skorobogatov, V.A., Stroganov, L.V., Kopeev, V.D., 2003. Geological Structure and Oil-and-gas Potential of Yamal. Nedra-Biznestsentr, Moscow, 343 pp. (in Russian)

Smirnov, A.S., 2014. Surficial evidences of fluid-dynamic processes of the Earth. The Young Permafrost Researchers of Russia Workshop No. 29. "A mystery crater on Yamal – what is the fact of the matter?" (Moscow, 28.11.2014) [Electronic resource]. URL: http://geoenv.ru/index.php/ru/novosti/seminary/284/763 (submittal date: 09.03.15).

SP 11-105-97, 2004. Geotechnical investigation of construction sites. Part VI. Guidance for conducting geophysical surveys. Gosstroi RF, 58 pp. (in Russian)

Trofimov, V.T. (Ed.), 1975. The Yamal Peninsula. Moscow University Press, Moscow, 280 pp. (in Russian)

Tsytovich, N.A., 1973. Mechanics of frozen soils. Textbook. Vysshaya Shkola, Moscow, 488 pp. (in Russian)

Vakhromeev, G.S., Erofeev, L.Ya., Zinchenko, V.S., Nomokonova, G.G., 1997. Rock Physics. Textbook. Izd-vo Tom. un-ta, Tomsk, 462 pp. (in Russian)

Vozhov, V.I., Surnin, A.I., 1982. Patterns of perennially frozen deposits distribution on the Siberian platform, in: Hydrogeology of Petroleum-bearing Areas of the Siberian Platform. SNIIGiMS, Novosibirsk, pp. 5–18. (in Russian)

Received March 23, 2015